



Contents lists available at ScienceDirect

Catalysis Today

journal homepage: www.elsevier.com/locate/cattod

Noble metal silicides catalysts with High stability for hydrodesulfurization of dibenzothiophenes

Kaixuan Yang^{a,b,1}, Xiao Chen^{a,1}, Zongxuan Bai^a, Changhai Liang^{a,*}^a State Key Laboratory of Fine Chemicals, Laboratory of Advanced Materials and Catalytic Engineering, School of Chemical Engineering, Dalian University of Technology, Dalian 116024, China^b Green Chemistry Centre, College of Chemistry and Chemical Engineering, Yantai University, Yantai 264005, China

ARTICLE INFO

Keywords:

Noble metal silicides
Deep HDS
Sulfur tolerance
DDS
Pathway

ABSTRACT

Development of highly efficient and long stable hydrodesulfurization (HDS) catalysts still is a great challenge for the refining industry. In this work, a series of intermetallic noble metal silicides supported by carbon nanotubes catalysts (Pt₂Si/CNTs, Rh₂Si/CNTs, and RuSi/CNTs) have been developed by chemical vapor deposition successfully, using dichlorodimethylsilane as Si source. These materials were used as efficient catalysts for the deep HDS of dibenzothiophenes (4,6-DMDBT and DBT) and performed high selectivity to the direct desulfurization pathway. The sequence of HDS activity over noble metal silicides catalysts is in keeping with the sequence of HDS activity of the corresponding metal catalysts, which is Pt₂Si/CNTs > Rh₂Si/CNTs >> RuSi/CNTs. In addition, the Pt₂Si/CNTs performed an excellent stability in 100 h stability testing for HDS of 4,6-DMDBT. Therefore, this sulfur-tolerant noble metal silicides could be as promising catalysts for the ultra-deep HDS of fossil-fuel.

1. Introduction

Removal of sulfur compounds from fossil-fuel and production of clean oil products is an inevitable trend and the development of highly efficient HDS catalysts would be a great challenge in the refining industry [1,2]. Traditional Ni(Co)Mo(W) sulfides HDS catalysts presented good HDS activity and stability in the process of gasoline and diesel oil refining during the implementation of relatively loose fuel oil sulfur emission standards (<500 ug/g) due to their low cost [2–4]. With the attention to environmental problems and increasingly stringent regulations on sulfur content in fuel oil, the technology of deep and ultra-deep desulfurization has aroused widely public concern gradually [5]. However, due to the large steric hindrance of dibenzothiophene and its alkylated derivatives, traditional Ni(Co)Mo(W) sulfide catalysts performed low activity for the deep HDS of these compounds in comparison with the HDS of thioether and its derivatives. Deep desulfurization of the fuels implies that the least reactive sulfur compounds must be converted, which requires the application of severe operating conditions and the use of especially active catalysts. Unfortunately, the HDS process with increasing temperature and pressure are just not enough to remove last traces of sulfur without undesired side reactions. Therefore,

in order to meet the increasingly stringent environmental requirements and further reduce the sulfur content in gasoline and diesel oil, the development of novel highly efficient deep HDS catalysts become the focus of scientific researchers.

Although supported noble metal catalysts are expensive and scarce, they have much better hydrogenation performances than those of conventional metal sulfides in HDS of dibenzothiophenes, which may be used in the second reactor of a deep HDS process [6–8]. However, the easy poisoning of the active sites by sulfur would be a major drawback, which reduce their lifetime dramatically [9,10]. Therefore, many researchers have done plenty of efforts to improve the sulfur tolerance of noble metal catalysts. Generally, the acidic supports were employed for supporting noble metal catalysts at HDS reaction since there are partial transfer of electrons from the metal to acidic sites in the supports, which would decrease the adsorption between noble metal and H₂S and improve the sulfur tolerance of noble HDS catalysts [11,12]. However, the fossil-fuel can be decomposed and isomerized over acidic supports, which not only decreases the yield of liquid product, but leads to the severe deactivation because of the coking. Therefore, another effective way to prepare the noble metal catalysts with high sulfur-tolerance should be developed.

* Corresponding author.

E-mail address: changhai@dlut.edu.cn (C. Liang).¹ These authors contributed equally to this work.<https://doi.org/10.1016/j.cattod.2020.08.027>

Received 22 January 2020; Received in revised form 16 July 2020; Accepted 24 August 2020

Available online 29 August 2020

0920-5861/© 2020 Elsevier B.V. All rights reserved.

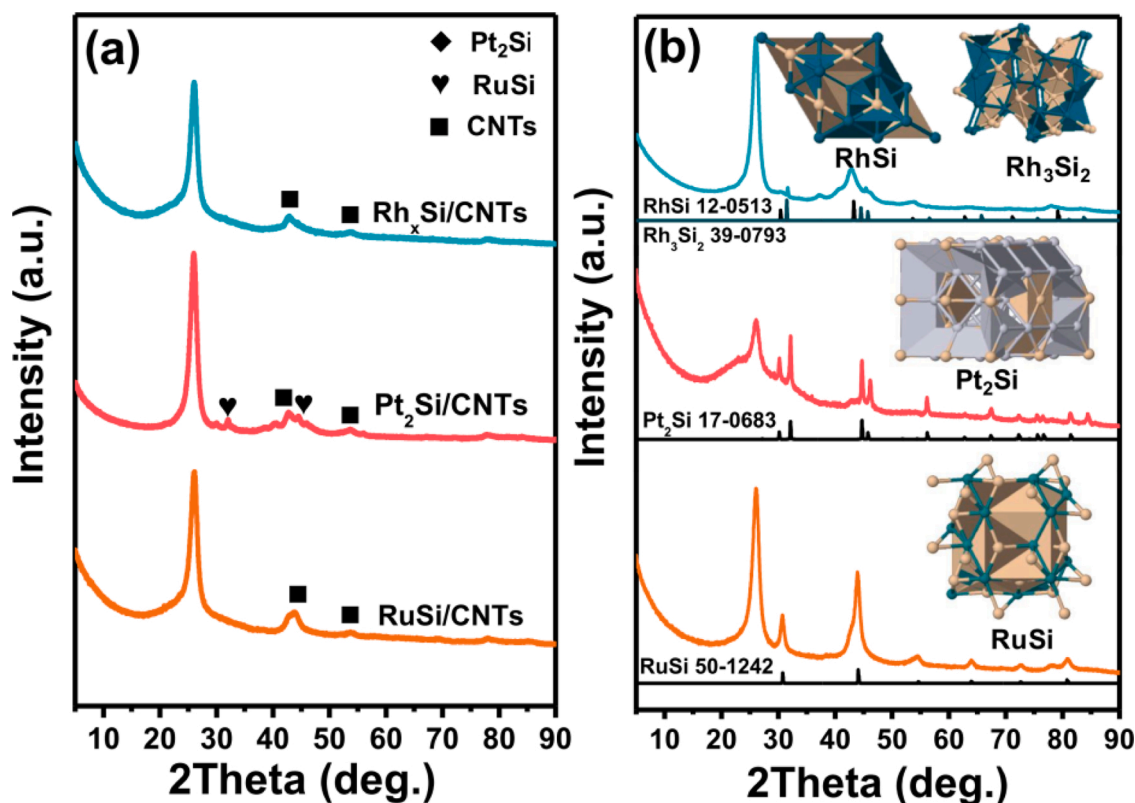


Fig. 1. XRD patterns of CNTs supported noble metal silicides with (a) 3 wt.% metal loading and (b) 10 wt.% metal loading. The inset images correspond to the construction of intermetallic noble metal silicides.

The combination of noble metals with metals or non-metallic elements to form alloys or intermetallic compounds can improve the sulfur tolerance of noble metal catalysts to some extent [13], which has already been confirmed by Pd-Pt, Pd-Au, and Pt-Ir bimetallic catalysts due to the synergistic effect [14–17]. Recently, the intermetallic compounds have shown excellent performances on the HDS reaction. Kanda et al. prepared a new Rh_2P catalyst, which exhibited excellent activity and stability for HDS reaction [18,19]. Richard et al. also prepared Pd-P and Ru-P catalysts with different phases, which showed high stability during the testing [20]. Similarly, Bussell et al. found that the Rh_2P/SiO_2 catalyst performed high stability during the 100 h HDS stability measurement and had higher sulfur-tolerance than the metallic Rh/ SiO_2 catalyst [21]. The Rh_2P/SiO_2 catalyst preferred the hydrogenation desulfurization (HYD) pathway for the HDS of dibenzothiophene (DBT), which was different from that of sulfide-Rh catalyst.

Interestingly, Searcy et al. studied the stability of intermetallic compounds in the presence of H_2S by chemical thermodynamics and found that transition metal silicides could tolerate much more H_2S than the corresponding phosphides [22]. In our previous research, density functional theory calculations (DFT) was also carried out to explore the relationship between the electronic structure and the origin of the efficient sulfur tolerance of metal silicides, which indicated that the S-poisoning process of the active sites was suppressed or strongly decelerated due to the special electronic structure in $NiSi_2$ [23,24]. However, the HDS activities of non-noble metal silicides catalysts were inferior in comparison with those of traditional Ni(Co)Mo(W) sulfide catalysts, despite the highly sulfur-resistant capability. Furthermore, a high S-tolerant and efficient noble metal silicide ($Pd_2Si/CNTs$) catalyst was developed, which showed good stability over an 80 h lift testing and performed 3-fold HDS activity than that over commercial Ni-Mo sulfide catalyst [25]. The previous research results give us enlightening for designing other highly efficient and good sulfur tolerant noble metal silicides catalysts for the ultra-deep HDS of fossil-fuel.

Table 1

Structural properties of CNTs and CNTs-supported noble metal silicides catalysts.

Sample	S_{BET} (m^2/g) ^a	d (nm) ^a	Metal loading (wt.%)	Particle size (nm)
CNTs	144	3.72	–	–
$Rh_xSi/CNTs$	146	3.72	2.86	2.49 ± 0.56
$RuSi/CNTs$	140	3.72	2.79	2.94 ± 1.10
$Pt_2Si/CNTs$	143	3.72	2.93	1.33 ± 0.32

^a BET surface area (S_{BET}) and average pore diameter (d) were determined by using N_2 adsorption-desorption isotherms measured at $-196^\circ C$.

Herein, a series of intermetallic noble metal silicides supported by carbon nanotubes catalysts ($Pt_2Si/CNTs$, $Rh_xSi/CNTs$, and $RuSi/CNTs$) have been developed and applied in the HDS of DBT and 4,6-DMDBT. The geometrical and electronic structures and HDS performances of intermetallic noble metal silicides catalysts have been investigated in-depth. The $Pt_2Si/CNTs$ catalyst has shown the highest HDS activity in comparison with the other noble metal silicides catalysts. Furthermore, the $Pt_2Si/CNTs$ catalyst has performed an excellent stability in the HDS of 4,6-DMDBT.

2. Experiment

2.1. Materials

All the chemicals were reagent grade and used without further purifications. $H_2PtCl_6 \cdot 6H_2O$, DBT, 4,6-DMDBT, and decalin were purchased from Sinopharm Chemical Reagent Co. Ltd. $RuCl_3 \cdot 3H_2O$ and $RhCl_3 \cdot 3H_2O$ were purchased from Aladdin Co. Ltd.

2.2. Catalysts preparation

Intermetallic noble metal silicides supported on carbon nanotubes (CNTs) catalysts were prepared by chemical vapor deposition (CVD) of dichlorodimethylsilane ($(\text{CH}_3)_2\text{SiCl}_2$) on M-O/CNTs (M = Pt, Rh, and Ru) samples in H_2 flow. Taking the preparation of $\text{Pt}_2\text{Si}/\text{CNTs}$ as an example, the Pt-O/CNTs precursor was firstly synthesized by impregnation the $\text{H}_2\text{PtCl}_6 \cdot 6\text{H}_2\text{O}$ in CNTs and then calcinated at 350°C for 2 h. Secondly, the Pt-O/CNTs precursor was loaded in a quartz boat and put into the middle of the horizontal quartz tube furnace, which was reduced at 350°C for 2 h with 30 sccm H_2 . When it reached the deposition temperature (500°C), $(\text{CH}_3)_2\text{SiCl}_2$ maintained at 0°C was carried into the quartz tube to deposit on the reduced Pt/CNTs sample for 1 h using H_2 (10 sccm) as the carrier. The exhaust gas was adsorbed by alkali solution. The $\text{Pt}_2\text{Si}/\text{CNTs}$ sample was cooled down to room temperature and passivated under O_2/Ar atmosphere for 12 h.

2.3. Catalysts characterization

X-ray diffraction (XRD) was carried out to analyze the structure and phase of catalysts, using a D/MAX-2400 diffractometer (Cu $\text{K}\alpha_1$ radiation, $\lambda = 0.15418$ nm) and operated at 40 kV and 100 mA. Analysis of element contents of Pt-Si, Rh-Si, and Ru-Si catalysts were carried out on an inductively coupled plasma optical emission spectrometer (ICP-OES). Nitrogen adsorption-desorption isotherms were constructed using the multi-points method at -196°C with an Autosorb IQ surface area and

pore size analyser. Transmission electron microscopy (TEM) and scanning transmission electron microscope (STEM) was performed by using a Tecnai G2 F30 S-Twin transmission electron microscope operating at 300 kV. Surface compositions and chemical state were investigated using X-Ray photoelectron spectroscopy (XPS) employing an ESCA-LAB250 (Thermo VG, USA) spectrometer with Al $\text{K}\alpha$ (1486.6 eV) radiation with a power of 150 W. The core level spectra were referenced as the neutral C 1s peak at 284.6 eV and were deconvoluted into Gaussian component peaks.

2.4. Catalytic testing

Typically, the catalytic HDS of DBT and 4,6-DMDBT over CNTs supported intermetallic noble metal silicides catalysts were conducted in a continuous flow fixed-bed reactor at 340°C and 3 MPa. Before the HDS properties testing, 0.1 g catalyst was reduced in situ in a 9 mm stainless steel tube by pure H_2 at 300°C for 2 h. During the reaction, the liquid feedstock including 1000 ppm 4,6-DMDBT or 3000 ppm DBT as reactant and decalin as inert solvent was pumped into the reactor. The reaction product with different reaction conditions after being condensed were collected at room temperature after the catalyst reached steady state and identified by Agilent 6890 N GC with 5973 MSD (HP-5 MS capillary column, 0.32 mm \times 0.25 μm \times 30 m), and analyzed by Agilent GC 7890A with FID (HP-5 capillary column, 0.32 mm \times 0.25 μm \times 30 m).

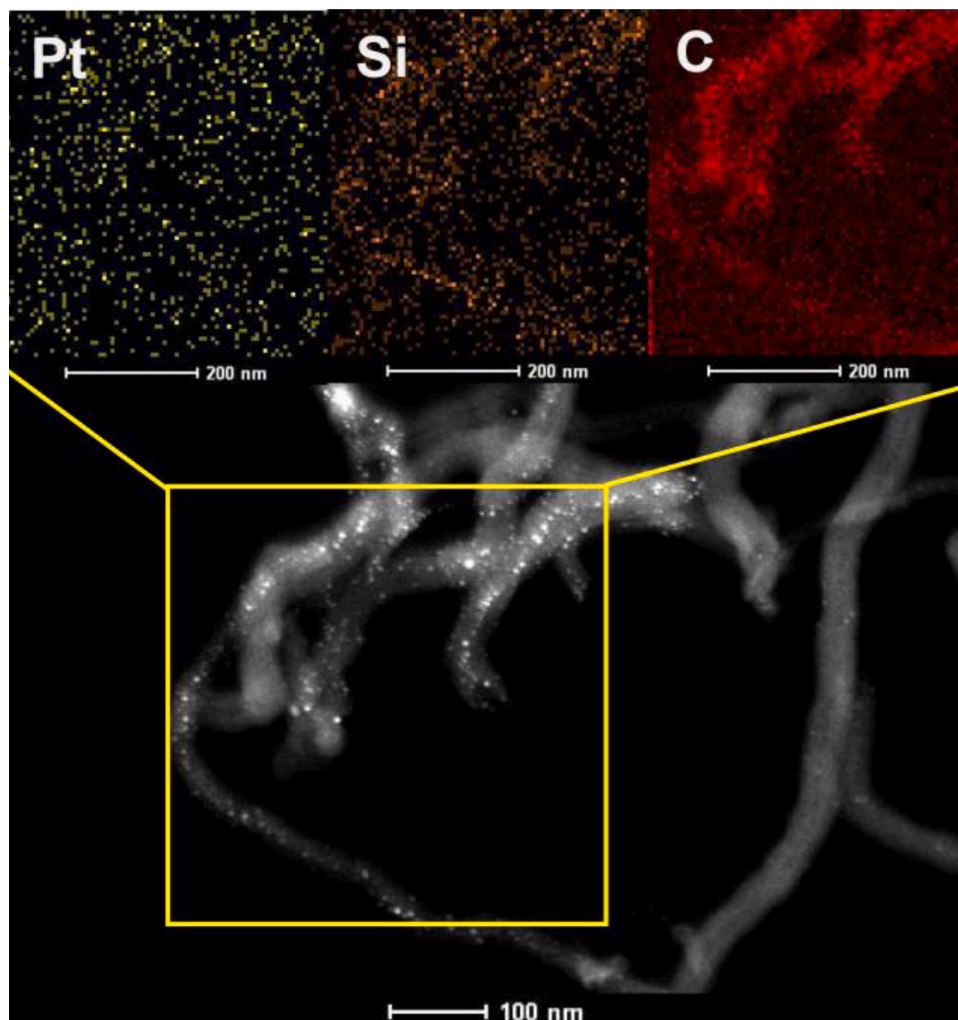


Fig. 2. STEM image and STEM-EDX element mapping images of $\text{Pt}_2\text{Si}/\text{CNTs}$ sample.

3. Results and discussion

3.1. Characterization of supported noble metal silicides catalysts

The structure and crystal phases of the as-prepared Pt₂Si/CNTs, Rh_xSi/CNTs, and RuSi/CNTs samples are confirmed by XRD patterns. For all the XRD patterns of the samples in Fig. 1, there are three same diffraction peaks at ca. 26.2°, 44.2°, and 54.0° corresponding to CNTs. In the XRD pattern of Pt₂Si/CNTs sample, there are two tiny peaks at 32.1° and 44.7°, which are corresponding to the (1, 1, 0) and (1, 1, 2) lattice planes of Pt₂Si (JCPDS # 17-0683). However, there is no peaks corresponding to noble metal or noble metal silicides in the XRD patterns of Rh_xSi/CNTs and RuSi/CNTs samples, which may be attributed to the low metal loading and low crystallinity. In order to find the direct evidence to prove the formation of noble metal silicides after CVD, Rh_xSi/CNTs, Pt₂Si/CNTs, and RuSi/CNTs samples with 10 wt.% metal loading are also prepared by CVD at the same reaction conditions. As shown in Fig. 1b, the peaks of Pt₂Si/CNTs and RuSi/CNTs samples match well with the standard pattern of Pt₂Si (JCPDS # 19-0893) and RuSi (JCPDS # 50-1242), respectively. It indicates that single-phase Pt₂Si and RuSi intermetallic compounds can be prepared successfully by CVD treatment. However, there are two phases including RhSi (JCPDS # 12-0513) and Rh₃Si₂ (JCPDS # 39-0793) in the Rh_xSi/CNTs sample. In addition, the crystal structure of Pt₂Si, RuSi, RhSi, and Rh₃Si₂ are inserted in Fig. 1b. Clearly, it shows that each Si atom is surrounded by metal atoms in those noble metal silicides intermetallic compounds. Similar with the intermetallic Pd₂Si sample, the active noble metal is partially isolated by Si atoms, which would lead to electronic structure modification and endow the metal with different catalytic performance [25]. Combined with the XRD results above all, the CVD method using (CH₃)₂SiCl₂ as the Si source is a general way to prepare supported noble metal silicides catalysts, especially for the preparation of single-phase noble metal

silicides.

Nitrogen adsorption-desorption isotherms of the CNTs support and M-Si/CNTs (M = Pt, Rh, and Ru) samples were measured to study the impacts of CVD treatment on the pore structure. All the BET surface area and average pore sizes of those catalysts are shown in Table 1. The specific surface area of the CNTs supported noble metal silicides catalysts show a slight decline compared with the CNTs support, except that of Rh_xSi/CNTs. There is no change on the average pore sizes of those catalysts. Besides, the ICP results in Table 1 also show that the metal loading of those catalysts still maintain at ca. 3 wt.% after the CVD treatment. These results indicate that there is almost no negative effect on the structure of support after the Si deposition.

In order to reveal the particle distribution and crystalline structure, the as-prepared Rh_xSi/CNTs, Pt₂Si/CNTs, and RuSi/CNTs samples were characterized by TEM and STEM-EDX measurements. The EDX element mappings in Fig. 2 and Fig. S1 confirm the elemental composition and indicate the presence of Si in these three noble metal silicides after the CVD treatment. Fig. 3 displays the TEM images and the particle size histograms of the as-prepared Rh_xSi/CNTs, Pt₂Si/CNTs, and RuSi/CNTs catalysts. As shown in Fig. 3, all these noble metal silicides nanoparticles are highly dispersed on CNTs and there is no apparent aggregation observed. The particle sizes of the noble metal silicides nanoparticles from statistical analysis is centered at 2.49 ± 0.56 nm, 1.33 ± 0.32 nm, and 2.94 ± 1.10 nm for the Rh_xSi/CNTs, Pt₂Si/CNTs, and RuSi/CNTs, respectively. As shown in Fig. 3b, the observed lattice spacing of the particle in Rh_xSi/CNTs is ca. 2.09 Å, which matches well with the (1, 1, 0) plane of RhSi with a tetragonal structure. Similarly, the measured lattice spacings of 2.03 Å and 2.35 Å are corresponding to the (1, 1, 2) plane of Pt₂Si, the (2, 0, 0) plane of RuSi, respectively. The results are corresponding to the XRD results, which further prove that highly dispersed noble metal silicides nanoparticles supported on CNTs were synthesized by CVD method successfully.

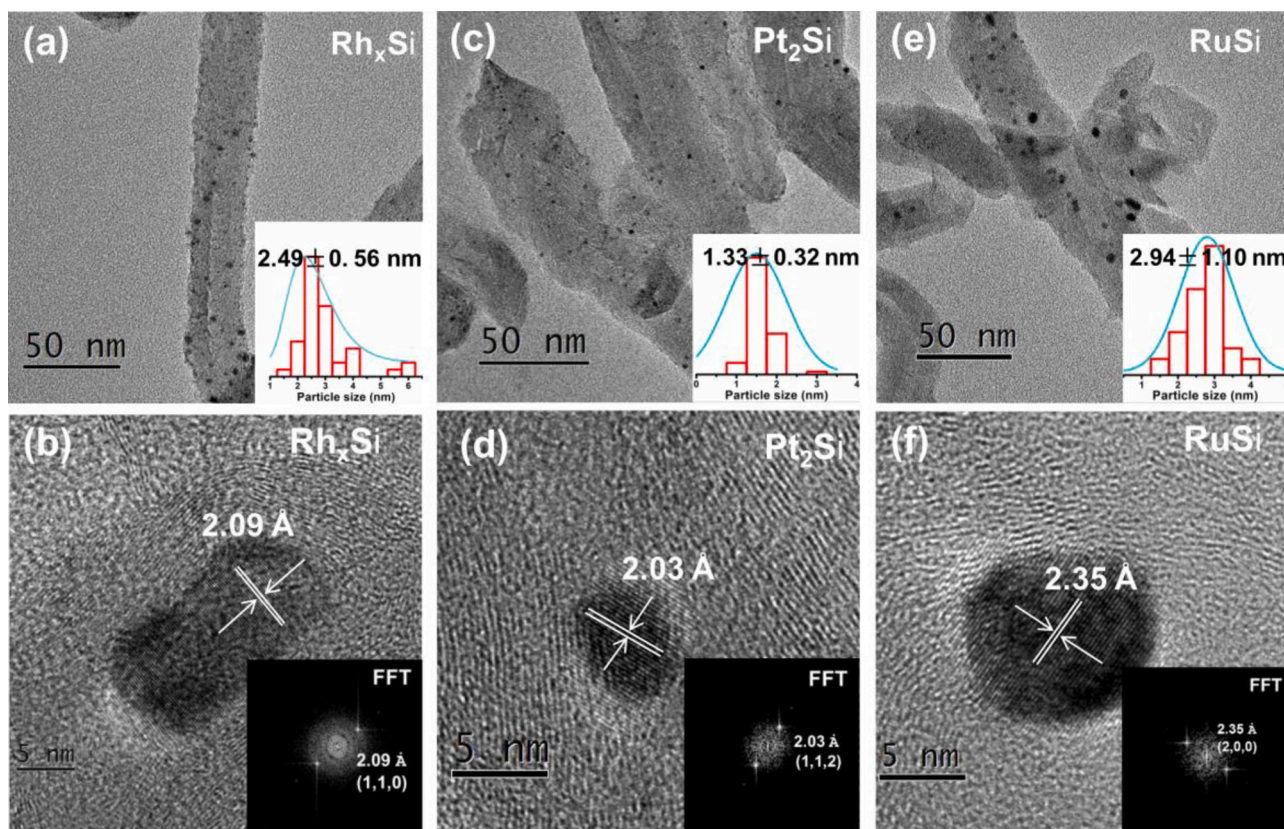


Fig. 3. TEM images and high-resolution TEM images of Rh_xSi/CNTs, Pt₂Si/CNTs, and RuSi/CNTs samples. The inset images correspond to particle size distribution and associated fast Fourier transformation, respectively.

The surface chemical properties of the Pt₂Si, RuSi, and Rh-Si samples are investigated by XPS (as shown in Fig. 4). There are two peaks at 74.0 eV and 78.1 eV belonging to 4f_{7/2} and 4f_{5/2} of Pt in PtO_x, which are derived from the slight surface oxidation of platinum silicide phase [26, 27]. The binding energy of the Pt 4f_{7/2} and Pt 4f_{5/2} at ca. 72.9 eV and 76.3 eV can be attributed to the Pt₂Si intermetallic compound, which are consistent with the reported by Morgan et al. [28,29]. In comparison with the XPS spectrum of metallic Pt 4f, the binding energy of Pt in Pt₂Si shifts to higher binding energy, which indicates that there is electron transfer from Pt to Si atoms [30]. As shown in Fig. 4f, the Rh peaks in spectrum of Rh 3d_{5/2} are at 307.1 eV and 307.6 eV, which are higher than the binding energy of metal Rh [31,32]. It indicates indirectly that the Rh combined with Si, leading to the higher binding energy of Rh. Besides, there are two peaks at 308.8 eV and 314.4 eV belonging to 3p_{3/2} and 3p_{5/2} of Rh in RhO_x, which are derived from the slight surface oxidation of Rh silicide phase [33,34]. Similarly, the Ru peak at 462.4 eV and 466.8 eV in spectrum of Ru 3p can be attributed to the Ru of RuSi and Ru of RuO_x, respectively [35,36].

3.2. HDS performances of supported noble metal silicides catalysts

The HDS performances of as-prepared noble metal silicides catalysts

and their corresponding noble metal catalysts are tested in the HDS of 4,6-DMDBT and DBT at different reaction conditions. Based on GC-MS analyses results, the reaction network of the HDS of 4,6-DMDBT over as-prepared noble metal silicides catalysts has been proposed, as shown in Scheme 1. There are five main products including 4,6-dimethylbiphenyl (4,6-DMBP), 4,6-dimethyltetrahydrodibenzothiophene (4,6-DM-TH-DBT), 4,6-dimethylhexahydrodibenzothiophene (4,6-DM-HH-DBT), 4,6-dimethylcyclohexylbenzene (4,6-DM-CHB), and 4,6-dimethylbicyclohexyl (4,6-DM-BCH). 4,6-DMBP is observed as the only product through DDS pathway. The intermediate products (4,6-DM-TH-DBT, 4,6-DM-HH-DBT, and 4,6-DM-CHB), and the fully hydrogenated product (4,6-DM-BCH) are observed as the products through HYD pathway. The selectivity to 4,6-DMBP (S_{DMBP}) is used for measuring the selectivity to DDS pathway, while $1-S_{\text{DMBP}}$ represents selectivity to HYD pathway. Normally, there are two different adsorption modes on the surface of active sites in the HDS of 4,6-DMDBT, which are vertical adsorption (adsorption to S atom) and horizontal adsorption (adsorption to benzene ring) [37,38]. The horizontal adsorption mode is positive to the HYD pathway, while the vertical adsorption mode for 4,6-DMDBT occurs on the edge sites, which would be beneficial to the DDS pathway [38]. Because of the steric hindrance of methyl, the HDS of 4,6-DMDBT over supported catalysts normally choose to go through HYD pathway but not

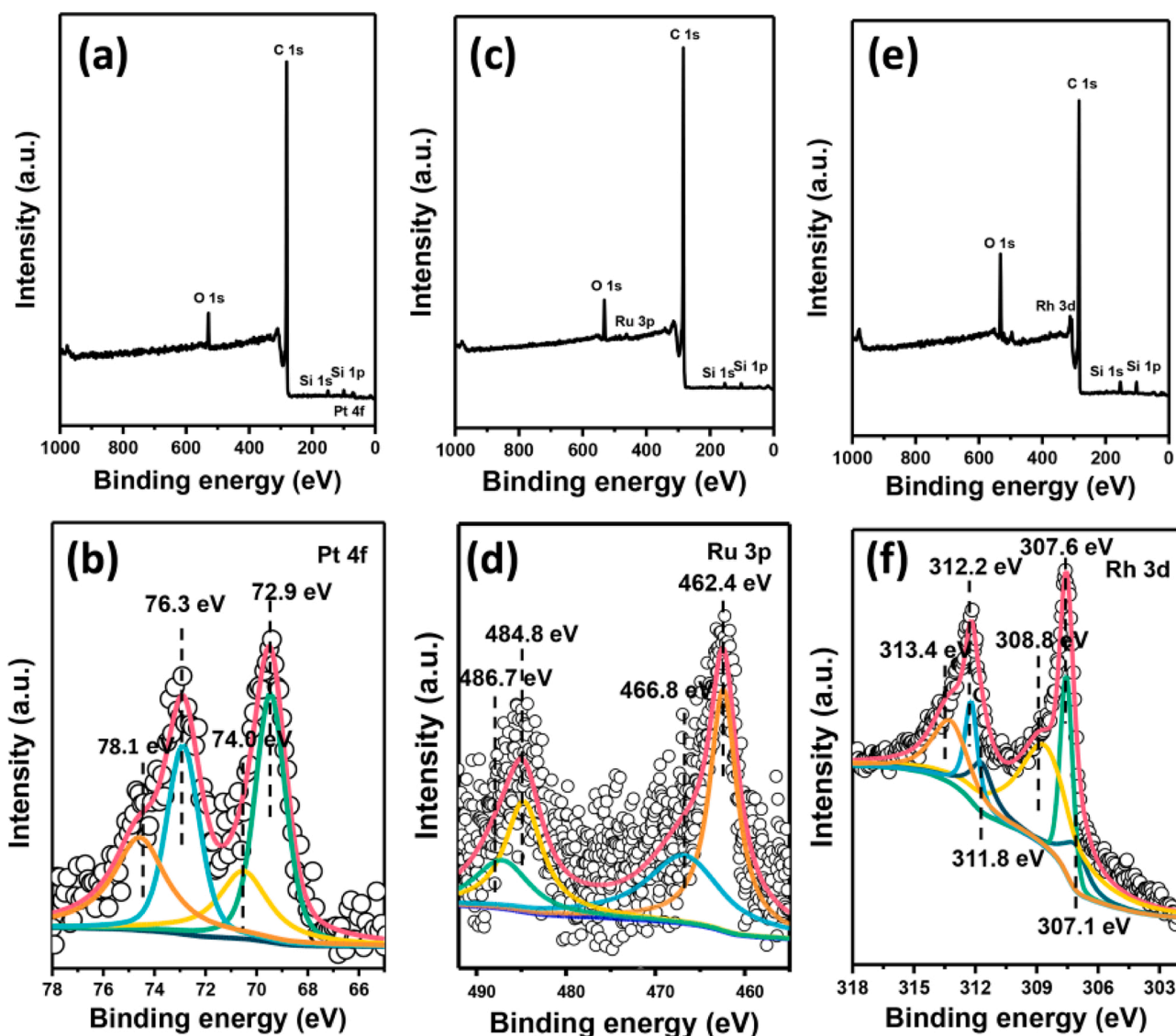
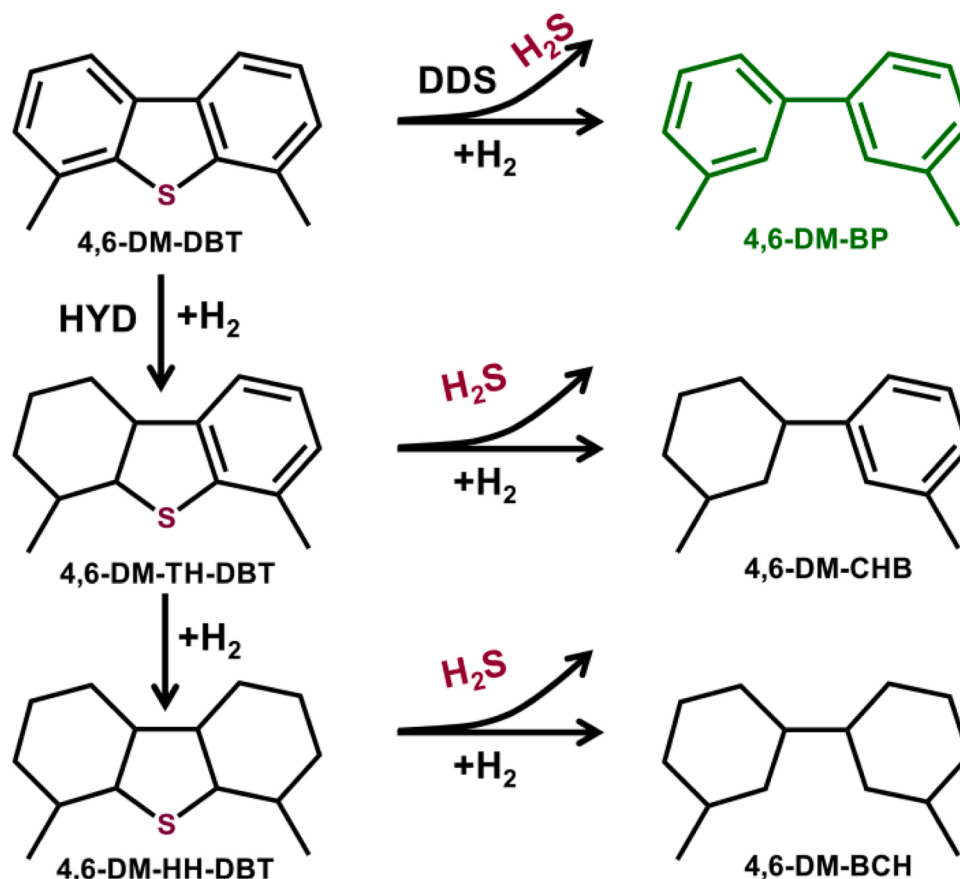


Fig. 4. XPS spectra of all elements in (a) Pt₂Si, (c) RuSi, and (e) Rh-Si, (b) Pt 4f region, (d) Ru 3p region, and (f) Rh 3d region in these samples.



Scheme 1. Reaction network of 4,6-DMDBT conversion over noble metal silicides catalysts.

DDS pathway, especially over the noble metal catalysts with a powerful hydrogenation capability of benzene ring.

Fig. 5 present the conversion of 4,6-DMDBT and the selectivity to DDS/HYD pathway over CNTs supported noble metal catalysts with different contact time at 340 °C and 3.0 MPa total pressure. It clearly demonstrates that the HDS activity decreases in the following order: Pt/CNTs > Rh/CNTs >> Ru/CNTs. The conversion of 4,6-DMDBT over Pt/CNTs and Rh/CNTs catalysts are 94.7 % and 43.2 % at the same contact time ($\tau = 0.74$ min), respectively, which are much higher than those over Ru/CNTs (< 5%). In addition, the selectivity to HYD reaction pathway over Pt/CNTs, Rh/CNTs, and Ru/CNTs are more than 85 % in the HDS of 4,6-DMDBT.

For the HDS of 4,6-DMDBT over CNTs supported noble metal

silicides catalysts, the $\text{Rh}_x\text{Si}/\text{CNTs}$ and RuSi/CNTs catalysts present almost no activity under 340 °C and 3 MPa. However, as shown in Fig. 5d, the $\text{Pt}_2\text{Si}/\text{CNTs}$ catalyst shows good activity for the HDS of 4,6-DMDBT. When the contact time closed to 0.6 min, the conversion of 4,6-DMDBT can reach to 50 %. The selectivity to 4,6-DMBP through the DDS route is as much as 40 %, which is much higher than that over the metal Pt/CNTs catalyst. A similar phenomenon occurred during HDS of 4,6-DMDBT over $\text{Pd}_2\text{Si}/\text{CNTs}$ catalyst, where the selectivity to DDS pathway was enhanced when the formation of intermetallic Pd_2Si [25]. Combining the geometric structure (Pt atoms isolated by Si atoms) and the electronic structure (electron transferred from Pt to Si) of intermetallic Pt_2Si , we can deduce that the modification of Si element to metallic Pt atoms would decrease the activation capacity of H_2 , which is negative

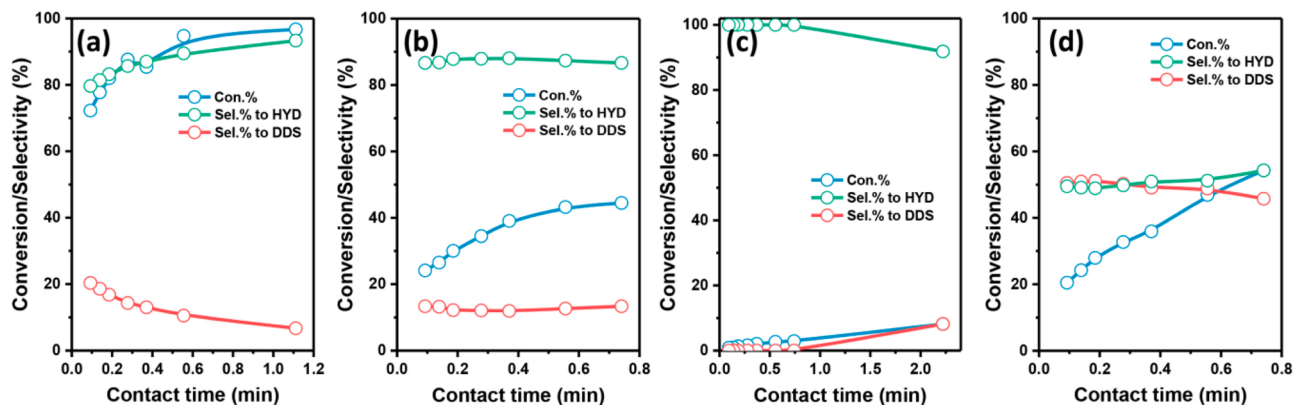


Fig. 5. 4,6-DMDBT conversion and selectivity to DDS/HYD over (a) Pt/CNTs, (b) Ru/CNTs, (c) Rh/CNTs, and (d) $\text{Pt}_2\text{Si}/\text{CNTs}$ catalysts. Reaction conditions: 340 °C, 3 MPa, and $\text{H}_2/\text{substrate} = 300$.

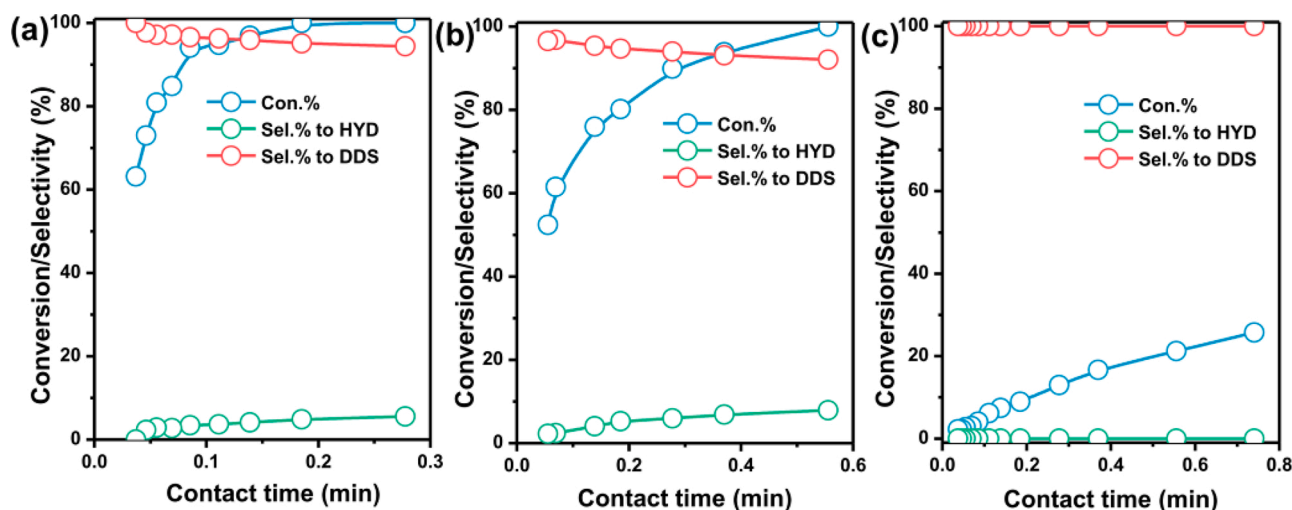


Fig. 6. DBT conversion and selectivity to DDS/HYD over (a) $Pt_2Si/CNTs$, (b) $Rh_xSi/CNTs$, and (c) $RuSi/CNTs$ catalysts. Reaction conditions: 340 °C, 3 MPa, and H_2 /substrate = 300.

Table 2

Catalytic performances of noble metal and metallic compounds catalysts for the HDS of DBT.

Catalysts	Con.%	Sel.% to DDS	Reaction conditions	Ref.
$Pt_2Si/CNTs$	100	95	340 °C, 3.0 MPa	This work
$Rh_xSi/CNTs$	100	92	340 °C, 3.0 MPa	This work
$RuSi/CNTs$	26	100	340 °C, 3.0 MPa	This work
Rh/SiO_2	30	76	275 °C, 3.0 MPa	[21]
Rh_2P/SiO_2	99	4	275 °C, 3.0 MPa	[21]
sulfided Rh/SiO_2	70	52	275 °C, 3.0 MPa	[21]
$Ru_2P/MCM-41$	100	26	348 °C, 3.0 MPa	[42]
$RuP/MCM-41$	99	27	348 °C, 3.0 MPa	[42]
RuP/SiO_2	–	60	325 °C, 3.0 MPa	[20]
Sulf. Ru/SiO_2	–	78	325 °C, 3.0 MPa	[20]
$Ru/MCM-41$	55	26	340 °C, 3.0 MPa	[42]
$Pt/AlM-I$	84	42	275 °C, 5.0 MPa	[7]

to the hydrogenation of benzene ring in 4,6-DMDBT, leading to the high selectivity to DDS pathway and preventing from the hydrogen consumption [25,39–41].

In addition, the $Rh_xSi/CNTs$, $Pt_2Si/CNTs$, and $RuSi/CNTs$ catalysts are used for the HDS of DBT. As shown in Fig. 6, the HDS activity of DBT over those three metal silicides catalysts are much higher than that of 4,6-DMDBT, because of the absence of methyl steric-hindrance effect. Among these catalysts, the $Pt_2Si/CNTs$ has the highest activity, which probably attribute to the high intrinsic activity of the corresponding metal Pt. The small particle size of the $Pt_2Si/CNTs$ is also beneficial to the HDS of DBT. The $RuSi/CNTs$ is the less active for the HDS of DBT. The sequence of HDS activity over the metal silicides catalysts is in keeping with the sequence of HDS activity over the corresponding metal catalysts, which indicates that the corresponding metal is the principal factor on the activity of metal silicides catalysts. Particularly noteworthy is that all these three kinds of metal silicide catalyst have superiorly high selectivity to DDS pathway during the HDS of DBT. As shown in Table 2, these noble metal silicides catalysts perform the highest selectivity to DDS under the similar conversion of DBT, in comparison with all the reported noble metal (Rh, Pt, and Ru) catalysts and noble intermetallic compounds (Rh_2P , Ru_2P , and RuP) catalysts [7,20,21,42].

The stability of $Pt_2Si/CNTs$ catalyst for the HDS of 4,6-DMDBT has been detected, as shown in Fig. 7. The conversion of 4,6-DMDBT is ca. 45%. There is no obvious deactivation even after 100 h stability testing. In addition, the selectivity to DDS pathway is almost unchanged, maintaining at ca. 40%. Comparing with the previous report that the metallic Pt catalyst with neutral support (Si-MCM-41) has shown a significantly deactivation during 8 h stability testing in HDS of DBT [43], the $Pt_2Si/CNTs$ catalyst has a high sulfur resistance during the HDS of 4,6-DMDBT. Combining the XRD and XPS results, the isolation effect and strong interaction between Pt and Si normally lead to a higher energy barrier for the combination between Pt (in Pt_2Si) and S, which could be the main reason for the excellent stability of $Pt_2Si/CNTs$ in the test.

4. Conclusions

In summary, intermetallic noble metal silicides supported by CNTs catalysts ($Pt_2Si/CNTs$, $Rh_xSi/CNTs$, and $RuSi/CNTs$) have been prepared by the CVD method successfully. Compared with the $Rh_xSi/CNTs$ and $RuSi/CNTs$, $Pt_2Si/CNTs$ catalyst shows the best HDS activity in the HDS of DBT and 4,6-DMDBT. These three catalysts perform superior selectivity to DDS pathway comparing with the corresponding noble metallic catalyst, which save the consumption of hydrogen to some extent. In

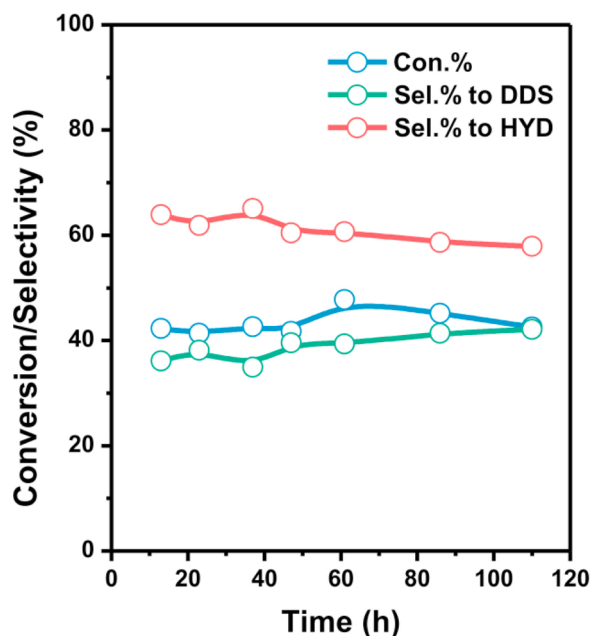


Fig. 7. Stability testing for 4,6-DMDBT conversion and selectivity to products over $Pt_2Si/CNTs$ catalyst. Reaction conditions: 340 °C, 3 MPa, and H_2 /substrate = 300.

addition, due to the active-site isolation by Si element and electron transfer between Pt and Si atoms, Pt₂Si/CNTs catalyst performs the excellent stability and sulfur resistance during the long-stream stable testing. Therefore, Pt₂Si/CNTs with highly efficient activity and good sulfur-tolerance as a novel inorganic material is a promising catalyst for the HDS of fossil-fuel.

Declaration of competing interest

The authors declare no competing interests.

CRediT authorship contribution statement

Kaixuan Yang: Data curation, Investigation, Writing - original draft. **Xiao Chen:** Conceptualization, Formal analysis, Writing - review & editing. **Zongxuan Bai:** Formal analysis, Software. **Changhai Liang:** Writing - review & editing, Supervision, Project administration, Funding acquisition.

Declaration of Competing Interest

The authors report no declarations of interest.

Acknowledgements

We thank the National Key Research & Development Program of China (2016YFB0600305), the Science and Technology Innovation Fund in Dalian City (2019J12GX028), Dalian Youth Science and Technology Star Project Support Program (2018RQ09), and the Fundamental Research Funds for the Central Universities (DUT18GJ206) for financial support.

Appendix A. Supplementary material

Supplementary data associated with this article can be found, in the online version, at <https://>

Appendix B. Supplementary data

Supplementary material related to this article can be found, in the online version, at doi:<https://doi.org/10.1016/j.cattod.2020.08.027>.

References

- [1] D. Hawksworth, F. Rose, *Nature* 227 (1970) 145–148.
- [2] T.G. Kaufmann, A. Kaldor, G.F. Stuntz, M.C. Kerby, L.L. Ansell, *Catal. Today* 62 (2000) 77–90.
- [3] D.A. Solís-Casados, L. Escobar-Alarcón, T. Klimova, J. Escobar-Aguilar, E. Rodríguez-Castellón, J.A. Cecilia, C. Morales-Ramírez, *Catal. Today* 271 (2016) 35–44.
- [4] A.E. Cruz Pérez, Y. Torrez Jiménez, J.J. Velasco Alejo, T.A. Zepeda, D.M. Frías Márquez, M.G. Rivera Ruedas, S. Fuentes, J.N. Díaz de León, *Catal. Today* 271 (2016) 28–34.
- [5] F. Tian, Q. Shen, Z. Fu, Y. Wu, C. Jia, *Fuel Process. Technol.* 128 (2014) 176–182.
- [6] F. Zhou, X. Li, A. Wang, L. Wang, X. Yang, Y. Hu, *Catal. Today* 150 (2010) 218–223.
- [7] X. Li, F. Zhou, A. Wang, L. Wang, Y. Wang, *Energy Fuels* 26 (2012) 4671–4679.
- [8] W. Shi, L. Zhang, Z. Ni, S. Xia, X. Xiao, *RSC Adv.* 4 (2014) 58315–58324.
- [9] T. Abdulkadir, A. Khalid, *Energy Fuels* 33 (2019) 2810–2838.
- [10] M.D. Argyle, C.H. Bartholomew, *Catalysts* 5 (2015) 145–269.
- [11] L. Zhang, W. Fu, Q. Ke, S. Zhang, H. Jin, J. Hu, S. Wang, T.D. Tang, *Appl. Catal. A Gen.* 433–434 (2012) 251–257.
- [12] S.A. Yashnik, G.A. Urzhuntsev, A.I. Stadnichenko, D.A. Svintsitskiy, A. V. Ishchenko, A.I. Boronin, Z.R. Ismagilov, *Catal. Today* 323 (2019) 257–270.
- [13] P. Vasudevan, J.G. Fierro, *Catal. Rev.* 38 (1996) 161–188.
- [14] C.O. Castillo-Araiza, G. Chávez, A. Dutta, J.A. de los Reyes, S. Nuñez, J.C. García-Martínez, *Fuel Process. Technol.* 132 (2015) 164–172.
- [15] A. Niquille-Röthlisberger, R. Prins, *Catal. Today* 123 (2007) 198–207.
- [16] A. Venezia, *J. Catal.* 215 (2003) 317–325.
- [17] A. Mansouri, N. Semagina, *Appl. Catal. A Gen.* 543 (2017) 43–50.
- [18] Y. Kanda, C. Temma, K. Nakata, T. Kobayashi, M. Sugioka, Y. Uemichi, *Appl. Catal. A Gen.* 386 (2010) 171–178.
- [19] Y. Kanda, Y. Matsukura, A. Sawada, M. Sugioka, Y. Uemichi, *Appl. Catal. A Gen.* 515 (2016) 25–31.
- [20] R.H. Bowker, M.C. Smith, B.A. Carrillo, M.E. Bussell, *Top. Catal.* 55 (2012) 999–1009.
- [21] J.R. Hayes, R.H. Bowker, A.F. Gaudette, M.C. Smith, C.E. Moak, C.Y. Nam, T. K. Pratum, M.E. Bussell, *J. Catal.* 276 (2010) 249–258.
- [22] A.W. Searcy, D.V. Ragone, U. Colombo, F. Donegani, *Chemical and Mechanical Behavior of Inorganic Materials*, Wiley-Interscience, 1970.
- [23] X. Chen, X. Liu, L. Wang, M. Li, C.T. Williams, C. Liang, *RSC Adv.* 3 (2013) 1728–1731.
- [24] X. Chen, C. Liang, *Catal. Sci. Technol.* 9 (2019) 4785–4820.
- [25] K. Yang, X. Chen, J. Qi, Z. Bai, L. Zhang, C. Liang, *J. Catal.* 369 (2019) 363–371.
- [26] T.H. Fleisch, G.W. Zajac, J.O. Schreiner, G.J. Mains, *Appl. Surf. Sci.* 26 (1986) 488–497.
- [27] S.J. Morgan, R.H. Williams, J.M. Mooney, *Appl. Surf. Sci.* 56 (1992) 493–500.
- [28] P.J. Grunthaner, F.J. Grunthaner, A.J. Madhukar, *J. Vac. Sci. Technol.* 20 (1982) 680–683.
- [29] G. Kiss, V.K. Josepovits, K. Kovács, et al., *Thin Solid Films* 436 (2003) 115–118.
- [30] D. Tyagi, S. Varma, S.R. Bharadwaj, *AIP Conference Proceedings* 1731, 2016, 080037.
- [31] A.M. Dennis, R.A. Howard, K.M. Kadish, J.L. Beare, J. Brace, N. Winograd, *Inorg. Chim. Acta Rev.* 44 (1980) 139–141.
- [32] Y. Baerl, P.F. Hedén, J. Hedman, M. Klasson, C. Nordling, K. Siegbahn, *Phys. Scr.* 1 (2007) 55–65.
- [33] J.P. Contour, G. Mouvier, M. Hoogewys, C. Leclere, *J. Catal.* 48 (1977) 217–228.
- [34] V.I. Nefedov, M.N. Firsov, I.S. Shaplygin, *J. Electron Spectrosc. Relat. Phenom.* 26 (1982) 65–78.
- [35] Q.M. Feng, P. Ma, Q.H. Cao, Y.H. Guo, J.J. Xu, *Chem. Comm.* 56 (2020) 269–272.
- [36] J.P.S. Badyal, R.M. Lambert, K. Harrison, C.C.A. Riley, J.C. Frost, *J. Catal.* 129 (1991) 486–496.
- [37] T. Kabe, A. Ishihara, Q. Zhang, *Appl. Catal. A Gen.* 97 (1993) L1–L9.
- [38] K. Chan, Y.K. Mi, K. Choi, H.M. Sang, *Appl. Catal. A Gen.* 185 (1999) 19–27.
- [39] X. Chen, J. Wang, K. Yang, C. Meng, C.T. Williams, C. Liang, *J. Phys. Chem. C* 119 (2015) 29052–29061.
- [40] X. Chen, M. Zhang, K. Yang, C.T. Williams, C. Liang, *Catal. Lett.* 144 (2014) 1118–1126.
- [41] K. Yang, X. Chen, G. Lafaye, C. Especel, F. Epron, C. Liang, *ChemistrySelect* 3 (2018) 11398–11405.
- [42] Q. Guan, C. Sun, R. Li, W. Li, *Catal. Commun.* 14 (2011) 114–117.
- [43] X. Li, F. Zhou, A. Wang, L. Wang, Y. Wang, *Energy Fuels* 26 (2012) 4671–4679.